

SCATTER CALCULATIONS IN RADIOGRAPHIC MODELLING

Andreas Schumm¹, Philippe Duvauchelle², Jérémy Giot², Joachim Tabary³, Roman Fernandez⁴,
Quentin Mistral⁵, Valérie Kaftandjian²

¹EDF R&D, 1 avenue du Général de Gaulle, 92141 Clamart, France

²INSA Lyon, Laboratoire CNDRI, Bât St-Exupéry, 25 Avenue Jean Capelle, 69621 Villeurbanne, France

³CEA LETI, MINATEC, F-38054, Grenoble, France.

⁴CEA LIST, F- 91191, Gif-sur-Yvette, France,

⁵Snecma, Site de Villaroche, Rond point Ree Ravaud, 77550 Moissy-Cramayel

Abstract

Scattered radiation is a fact of life in industrial radiography, and as such must also be taken care of in computer models for industrial radiography. The French national research project "RADIOLA" aims to integrate the key components of three existing computer codes (VXI: Virtual X-ray Imaging, Sindbad and Moderato) into the CIVA platform and provides several means to calculate scatter predictions, depending on the configuration at hand.

For high wall thicknesses, such as those typically encountered in nuclear applications, a traditional Monte Carlo scatter model is available, which provides reliable results at the expense of computation time. For components with smaller wall thicknesses, where first order scattering is dominant, an analytical approach is available, which is particularly well suited for aerospace applications.

We present and illustrate both approaches, compare their respective application domains, and conclude with a proposal for a hybrid model which attempts to provide n-th order scatter predictions, which could be a computationally effective approach for intermediate wall thickness ranges.

1. Introduction

Radiographic modeling for small wall thicknesses, where scattered radiation can be neglected, is mainly a problem of fast ray-tracing to extract path lengths in a CAD-defined geometry between a source point and a film pixel. For higher wall thicknesses, where scattered radiation represents a dominant part of the total radiation incident on the film, however, a reliable scatter prediction model is a key requirement for any modeling code.

For constant wall thicknesses, tabulated and interpolated build-up values are a straightforward and pragmatic solution. Scatter predictions for CAD-defined geometries with variable wall thicknesses, on the other hand, require a more advanced model. The traditional approach, implemented in most available codes [1] [2] [3], uses a Monte Carlo model to trace the path of each photon emitted at the source, propagated through the part geometry, until it either reaches the film, dies in an absorption event, or exits the part in a direction in which it can not intersect the film (if scattering in the ambient medium is neglected). Monte Carlo particle transport simulations are inherently precise, provided that the cross section data is precise and a sufficient number of events have been simulated to obtain reliable statistics. The approach can simulate all types of scatter events (Compton, Rayleigh, Pair Production), at arbitrary order. The prize of this versatility is high computation cost.

If higher order scattering events are not necessary (because the wall thickness at hand produces dominantly lower order scattering), alternative analytical approaches [4] [5] [6] [7] provide a faster alternative.

In this paper, we will describe analytical methods for scattering calculation developed in the VXI code (INSA), including the 3D sampling needed for such methods.

Results thus obtained will be compared to two Monte-Carlo based codes: MODERATO (EDF) and SINDBAD (CEA-LETI).

The current version of CIVA partially integrates developments done in Radiola's project. Until today only the simulation of scattered radiation computed from the Monte-Carlo approach is available [8].

2. Theory-principle

When an object is irradiated by an X-rays beam, photon-matter interactions, such as for example Compton (or incoherent) or Rayleigh (or coherent) scattering or photoelectric effect, occurs along the X-ray path. These interactions may provide secondary photons which may be either a useful or a parasite signal, depending on the experiment you are interested in. Taking into account x-ray scattering is then very important because it contributes of a non-neglecting part on the detector response.

Computing analytical scattered radiation consists in calculate on the detector the contribution of all interaction (scattering) points inside the tested object, according to the physics laws driven by the interaction process.

In practice, the first and crucial step of the computation is the 3D sampling of the scattering objects. In the next paragraph, we will present three different methods allowing such a computation. For now, assuming the sampling is already done, the second step consists in calculating the photons number arriving on each pixel of the detector after scattering from each point of the object, i.e. the 3D sampling. This step is done combining a ray-tracing algorithm and physical laws describing these phenomena. Figure 1 shows the principle of this computation.

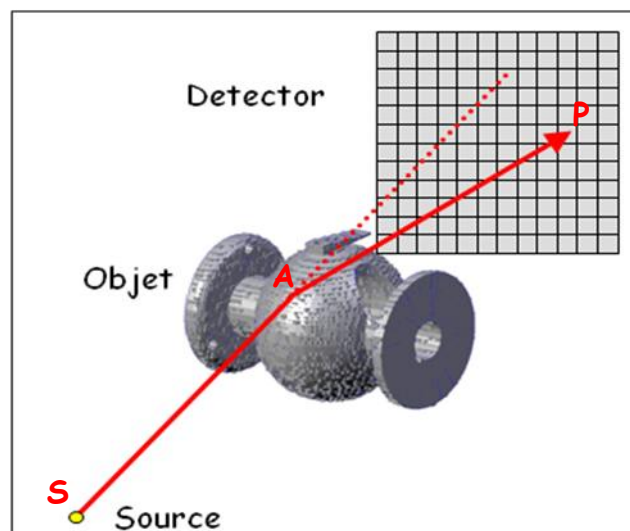


Figure 1: Principle scheme of the X-ray scattering

For the Compton scattering, we use the well-known Klein-Nishina model refined by the incoherent scattering function S . For the Rayleigh scattering, we use the Thomson model with the atomic form factor F . VXI uses the EPDL97 database for both the attenuation coefficients and the S and F functions, while

Moderato relies on an extraction of the MCNP data base for the form factor and scattering functions for this particular study. Sindbad uses the EGS-Nova data.

The number of photon arriving on a pixel P , resulting from the source S and passing by a scattering point A can be written:

$$N_P = N_0 \times \frac{S_A}{SA^2} \times \left(\frac{d\sigma}{d\Omega} \right)_{Scattering} \times \frac{\rho \cdot N_A}{M} \times L_A \times S_P \times \frac{\overrightarrow{AP} \cdot \overrightarrow{n_{\omega_v}}}{AP^3} \times e^{-\left(\sum_{SA} \mu_i \epsilon_{0_i} \vec{x}_i + \sum_{AP} \mu_j \epsilon_{d_j} \vec{x}_j \right)}$$

Or, remarking than $V = S_A \cdot L_A$

$$N_P = N_0 \times \frac{1}{SA^2} \times \left(\frac{d\sigma}{d\Omega} \right)_{Scattering} \times \frac{\rho \cdot N_A}{M} \times V \times S_P \times \frac{\overrightarrow{AP} \cdot \overrightarrow{n_{\omega_v}}}{AP^3} \times e^{-\left(\sum_{SA} \mu_i \epsilon_{0_i} \vec{x}_i + \sum_{AP} \mu_j \epsilon_{d_j} \vec{x}_j \right)} \quad (1)$$

Where:

N_0 is the photons number per solid angle unit;

$\frac{S_A}{SA^2}$ the solid angle under which the voxel associated to a scattering point is seen;

$\left(\frac{d\sigma}{d\Omega} \right)_{Scattering}$ the atomic scattering cross section (for Compton or Rayleigh);

$\frac{\rho \cdot N_A}{M} \times V$ the number of electrons inside the scattering volume V ;

$S_P \times \frac{\overrightarrow{AP} \cdot \overrightarrow{n_{\omega_v}}}{AP^3}$ the solid angle under which the pixel is seen;

$e^{-\left(\sum_{SA} \mu_i \epsilon_{0_i} \vec{x}_i + \sum_{AP} \mu_j \epsilon_{d_j} \vec{x}_j \right)}$ the attenuation term inside the object, from point source S to pixel P , passing scattering point A .

3. 3D Sampling methods

The 3D-sampling of scattering objects is an essential aspect for well estimate scattering contribution. 3D-sampling, in the aim to compute analytical scattered, can be divided in two families:

- The geometric methods

Sampling is done taking into account the shape of the object only. We will present two geometry-based methods: the first one provides a random uniform sampling while the second, generates a shape-adaptative sampling. These methods allow computing the first order only.

- The physic-geometric coupled methods

We have tested another method using a Monte-Carlo code to provide the scattering points. This method allows computing n^{th} order scattering.

a. Random sampling

To obtain scattering points, we first determine a bounding box of the object. After that, we randomly generate points inside this bounding box. Testing if the point is inside or outside the object allows keeping or rejecting it (figure 2). The volume associated to each point (required in equation 1) is calculated dividing the total volume of the object by the number of retained scattering points.

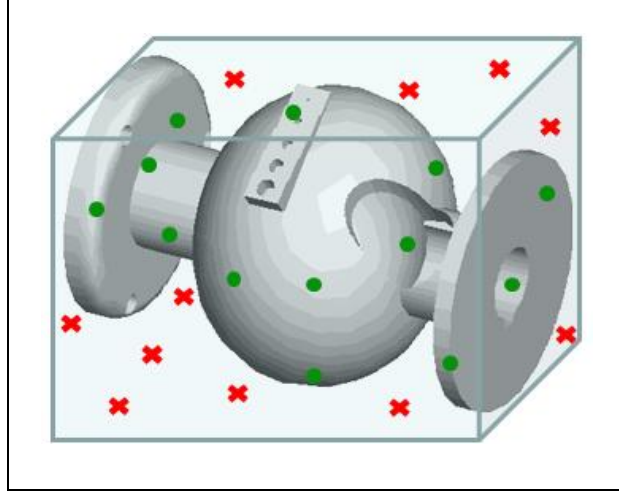


Figure 2: Principle illustration of the random sampling

This method is very simple to implement, low time-consuming and user friendly because the only input for the algorithm is the points number to use. On the other hand, this value is not easy to know a priori but this method allows an online and automatic deduction of the best value, according to criteria measurable on the scattered image.

Finally, it can be noticed that this method is badly adapted for the objects which present strong variations of thickness because the number of points in the thin parts is too low comparing to the thicker parts.

Figure 3 shows the sampling obtained on a 10 mm thickness iron plate in two directions of space.

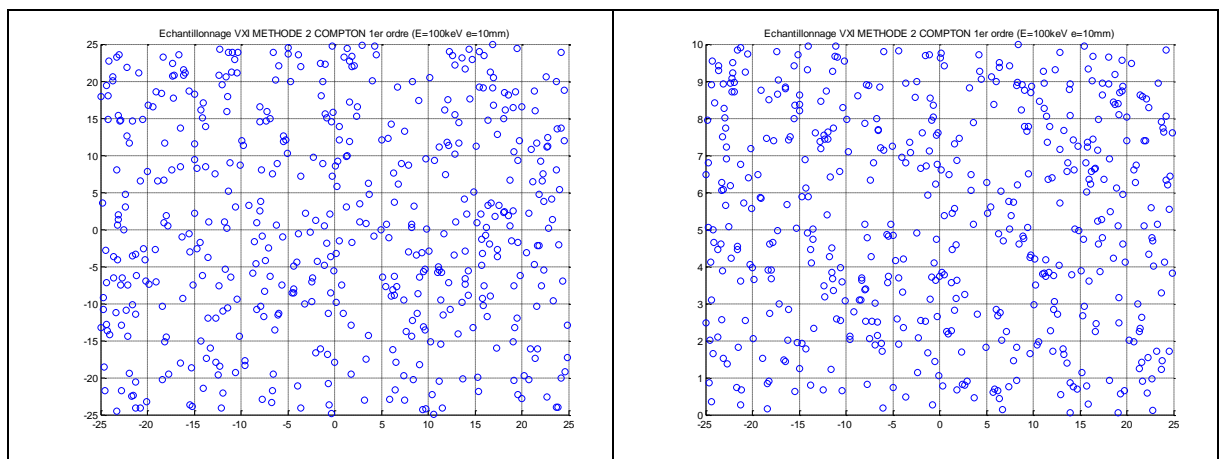


Figure 3: 3D sampling obtained with a 10 mm thickness iron plate. On the left, view is represented in the plan of the plate (50 mm x 50 mm), on the right, in the depth direction (10 mm thickness).

b. Octree-based adaptative sampling method

This method, based on the octree principle, has been extended, optimized and specifically developed for our application. Starting from a bounding box of the object we want to sample, we divide this box in two in the three directions of space. We then obtain eight voxels. We reproduce recursively this space division

for each voxel previously created, until it is completely under the object surface. This is the octree-subdivision method illustrated on figure 4.

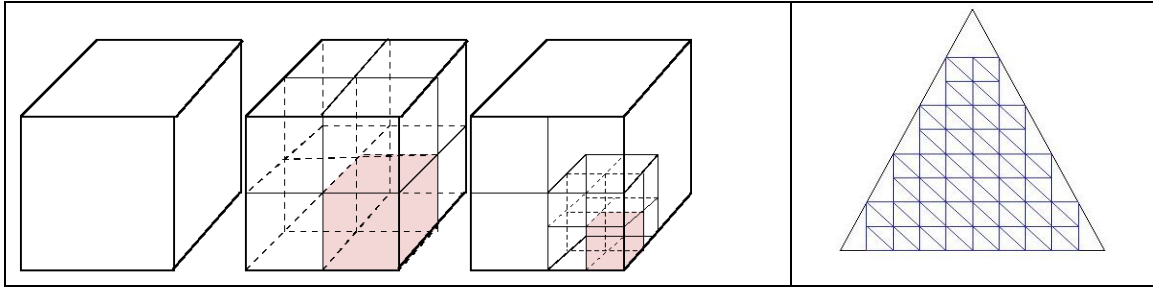


Figure 4: Illustration of the Octree-subdivision method

This method provide same-size aligned voxels whose volumes sum is necessary under-estimated in comparison to the real object volume. This may cause under-estimated scattering evaluation (see equation 1). Furthermore, the aligned voxels may generate some sampling artefacts on the simulated image.

In order to resolve these potentials problems, we optimized and developed the octree method by adding some specific improvements, in regard to our application. First, we accept some voxel even if they are not completely under the object surface. The total sum of the volume voxels will then tend to the exact scattering volume. Second, to avoid sampling artefacts, we divide each voxel by a random value chosen in the range from 1 to 2. Figure 5 illustrates the principle of this method and gives an example of a complex-geometry object (fan).

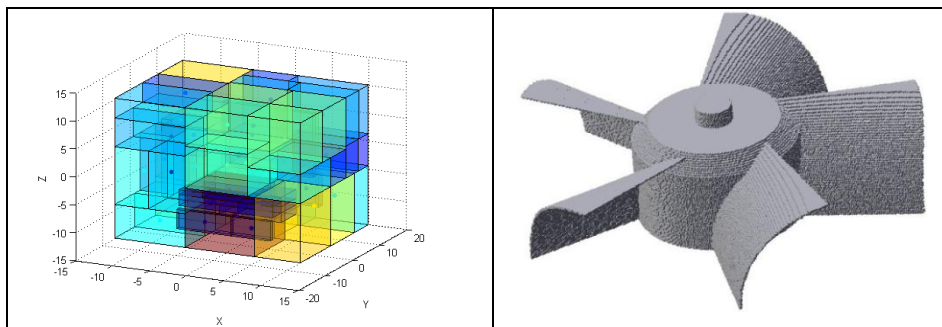


Figure 5: Illustration of the optimized Octree-subdivision method for scattering computation. On the left, we can see the different sizes and shapes of the voxels. On the right, a test of this algorithm applied on a realistic object presenting large thickness variations. The algorithm needs 10 seconds to generate about 125000 voxels.

This method is more difficult to implement than the previous one due to the recursive algorithm. Furthermore, parameters used by this method could not be trivial to set. On the other hand, this method gives excellent results, with low sampling noise, even on complex geometry and with a limited voxels number.

c. Monte-Carlo sampling

To perform such a sampling, we use a Monte Carlo code which generates a set of points from the geometrical configuration, taking into account physical laws for both attenuation and scattering. For each interaction point, we keep the incident energy of the photon, its direction, the type of interaction as well as the order of scattering. These information are needed to compute Compton and Rayleigh contribution.

This method is rather difficult to implement and time consuming for generating scattering points, especially for complex geometry. Besides this aspect, this method gives an important sampling noise. The

strength of this method lies in the fact that it can supply multiple scattering contributions faster than a Monte-Carlo code could give (from a few minutes to few hours depending on the points number and the complexity of the object).

Figure 6 illustrates the spatial distribution of generated points with 100 and 300 keV photons energies and an iron plate 30 mm in thickness. We choose here to keep the Compton first order only. On the example of the figure 7, we used an iron plate 10 mm in thickness and 100 keV photons energy. All the scattering orders for Compton effect have been kept here.

4. Simulation parameters

The 3D scene chosen to carry out our simulations is represented figure 8. Results presented section 5 have been obtained with this configuration.

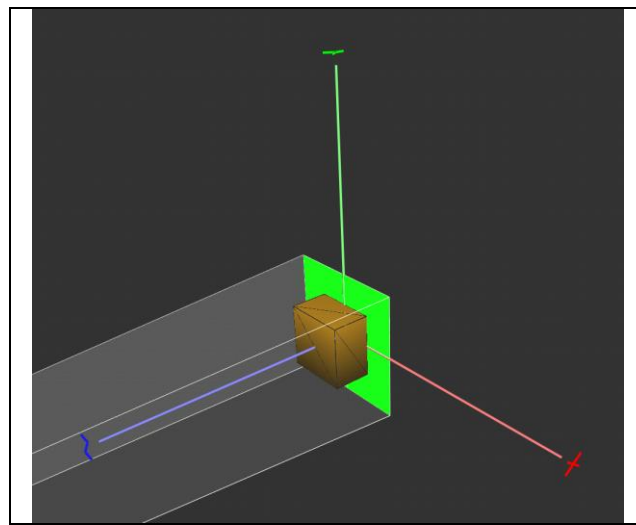


Figure 8: 3D arrangement used for simulations. Object is represented in brown, detector in green. Source is on the left (in the direction of the grey beam) but doesn't appear on the figure.

The point source is placed at a distance of one meter from the detector in green on the figure. The latter is an ideal detector (efficiency one) with 200x200 pixels, 0.5x0.5 mm² each. The object is an iron square plate 50 mm side and 10 or 30 mm in thickness, depending on the configuration studied. The object is placed against the detector, just in front of it. The source beam irradiate the all the detector and then the object. Finally, X-ray beam used is monochromatic and the photons energy is set at 100 keV or 300 keV.

In this way, we test four different configurations mixing plate thickness and photon energy:

- 100 keV/10 mm
- 100 keV/30 mm
- 300 keV/10 mm
- 300 keV/30 mm

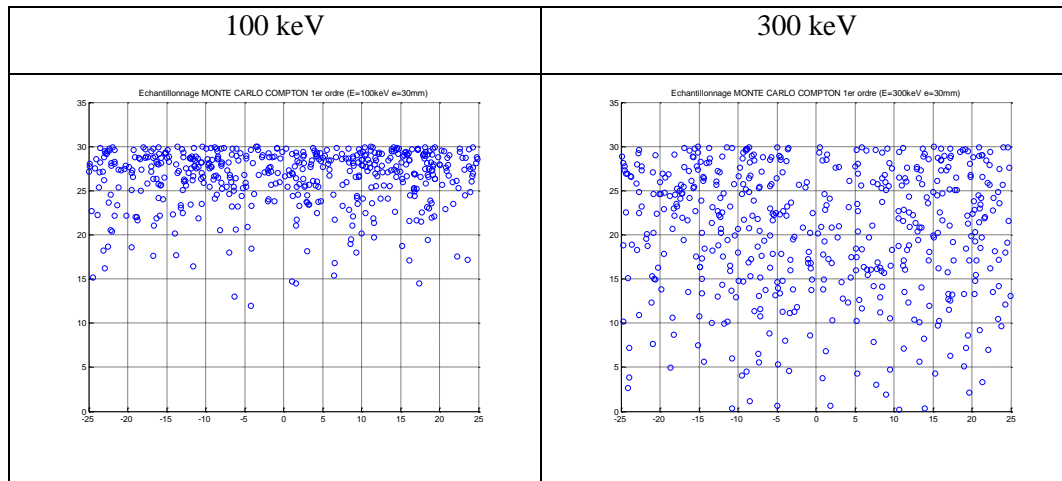


Figure 6: Scattering points geometric distribution. The object is a 30 mm thickness iron plate. On the left, photons energy is set at 100 keV, on the right at 300 keV.

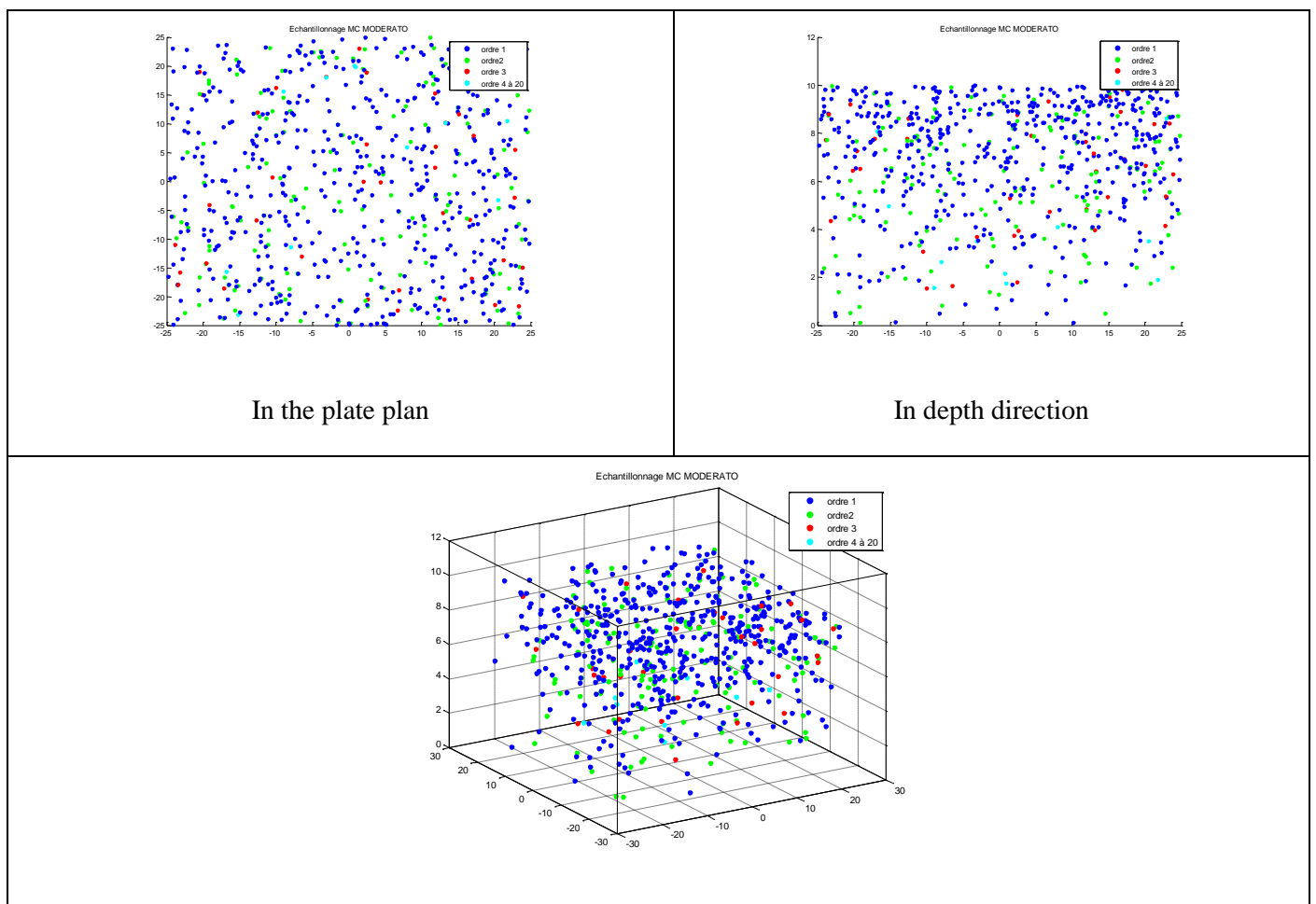


Figure 7: 3D distribution scattering points for scattering orders from 1 to 20. The object is a plate 10 mm in thickness irradiated with a 100 keV photons beam.

5. Results and discussion

Figure 9 resumes the results for Sindbad, Moderato, and VXI with the three sampling techniques qualitatively in terms of scatter images.

Noise observed in the VXI's images is due to 3D sampling while the noise obtained with Monte-Carlo methods (Moderato and Sindbad) come from the photonic noise inherent of the latter. In both cases, increasing the number of sampling points or the number of photons reduce the noise. In these examples, VXI work with 50000 sampling points while Sindbad and Moderato use 10^9 photons.

We notice that at 100keV, VXI converges faster for both thicknesses, and in particular at 30mm. Both Monte-Carlo codes show considerably higher noise than the analytical model. With variance reduction disables, Moderato also converges slightly slower than Sindbad.

At 300keV, the results are less obvious. Sampling technique 2 provides the best convergence, although the advantage with respect to a slower Monte Carlo model does not appear in these images, with the simulation parameters chosen in this example.

When using sampling techniques, it can be notice that the scattering points number must be adjust in regard to the volume of the sample. Thus, as we have chosen to work here with constant sampling points, results obtained at 30 mm seem to converge more slowly.

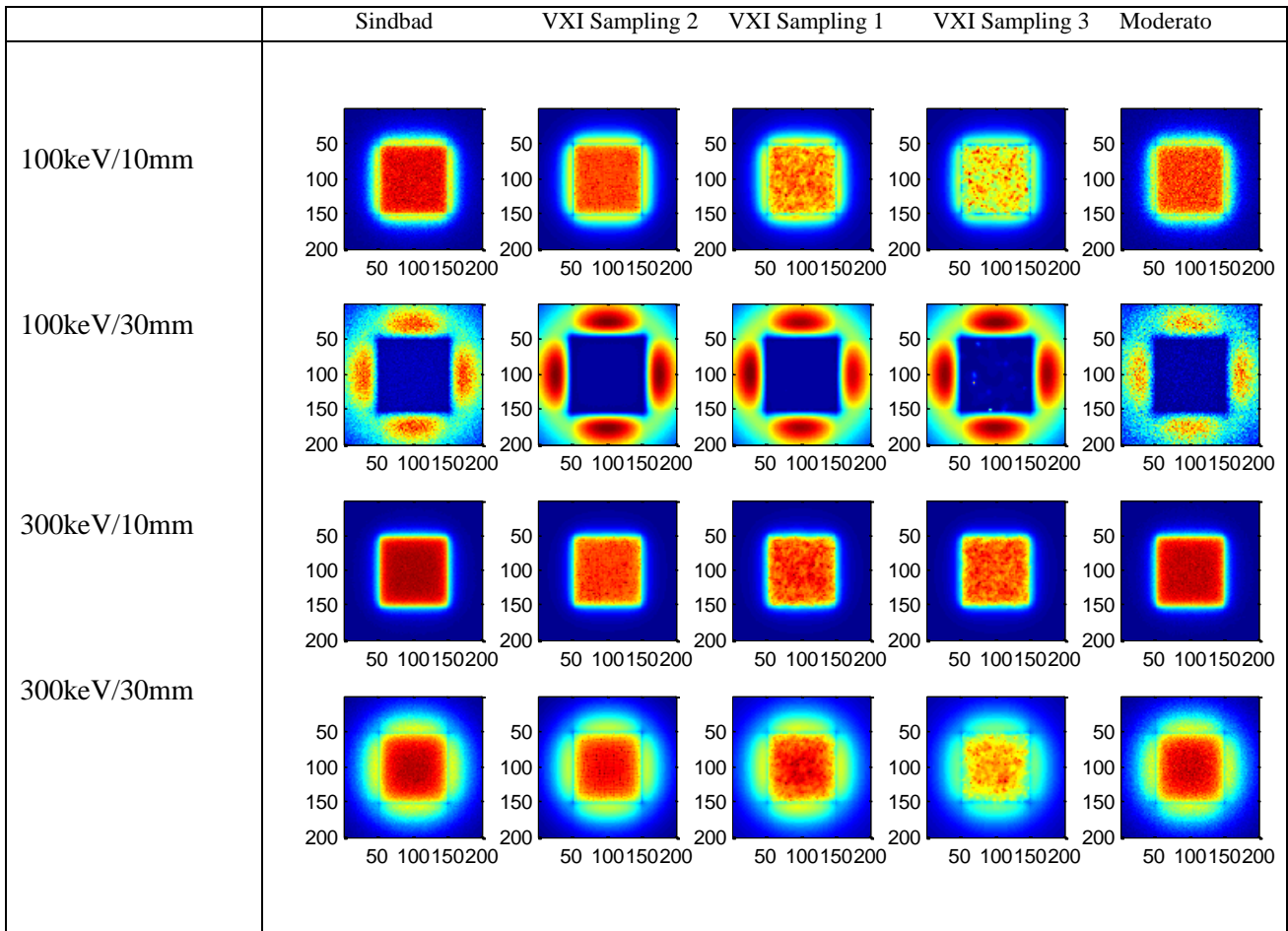


Figure 9: scatter images for Sindbad, VXI with three sampling techniques and Moderato

Figure 10 provides a quantitative analysis of the results in terms of scatter profiles. At 100 keV, the first order scattering results provided by VXI and the Monte Carlo models show significant differences. This can be explained by the fact that the different codes use different database (See section 2). The Monte Carlo profiles are quite noisy; calculations with a larger number of photons are required to obtain a quantitatively exploitable result. At 100keV/30mm, the VXI results are very smooth, independently of the sampling method chosen.

At 300 keV, differences between VXI and Sindbad or Moderato are low. The shape of the scatter profile is well predicted, the noise inherent to each model is clearly apparent. From these profiles, the results are roughly the same, even if the Monte-Carlo sampling shows a higher noise.

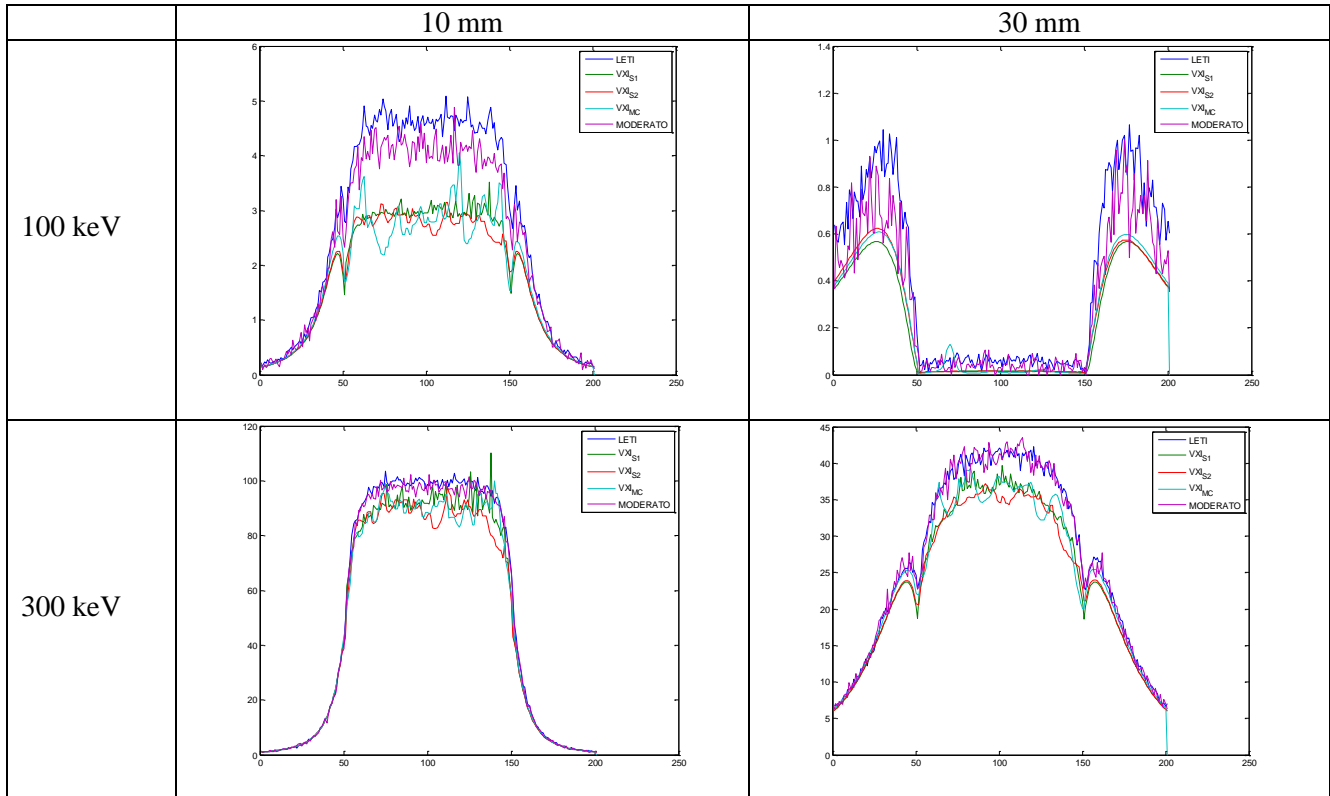


Figure 10: Scatter profiles for Sindbad, Moderato and VXI with three sampling techniques

As shown in figure 11, Monte-Carlo sampling allows for multiple scatter calculations. It is interesting to calculate the contribution of each scatter order. A quantitative analysis is possible from figure 12, which traces the profile for first, second, third and higher order scatter events, as well as the total scattering. For this particular geometry, the sum of first and second order scattering is close to the total scattering, suggesting that 3rd and higher order events can be neglected. The graph also shows the relatively high sampling noise of the Monte-Carlo sampling approach. Simulation's user must find a compromise between an adapted number of sampling points and a reasonable computing time.

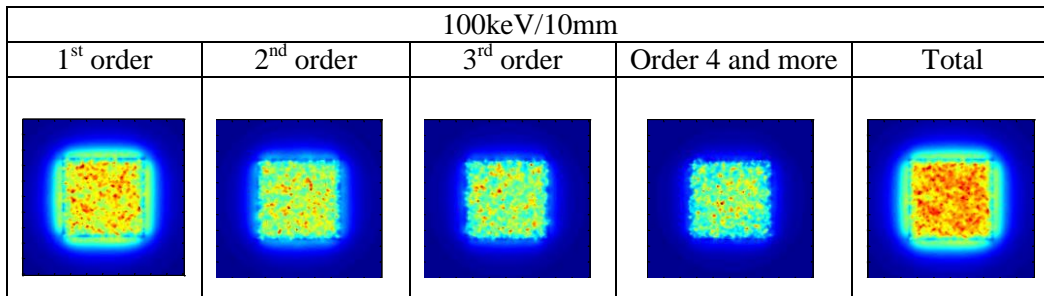


Figure 11: Scatter images for VXI and Monte-Carlo sampling technique. Images show the contribution of different scattering orders.

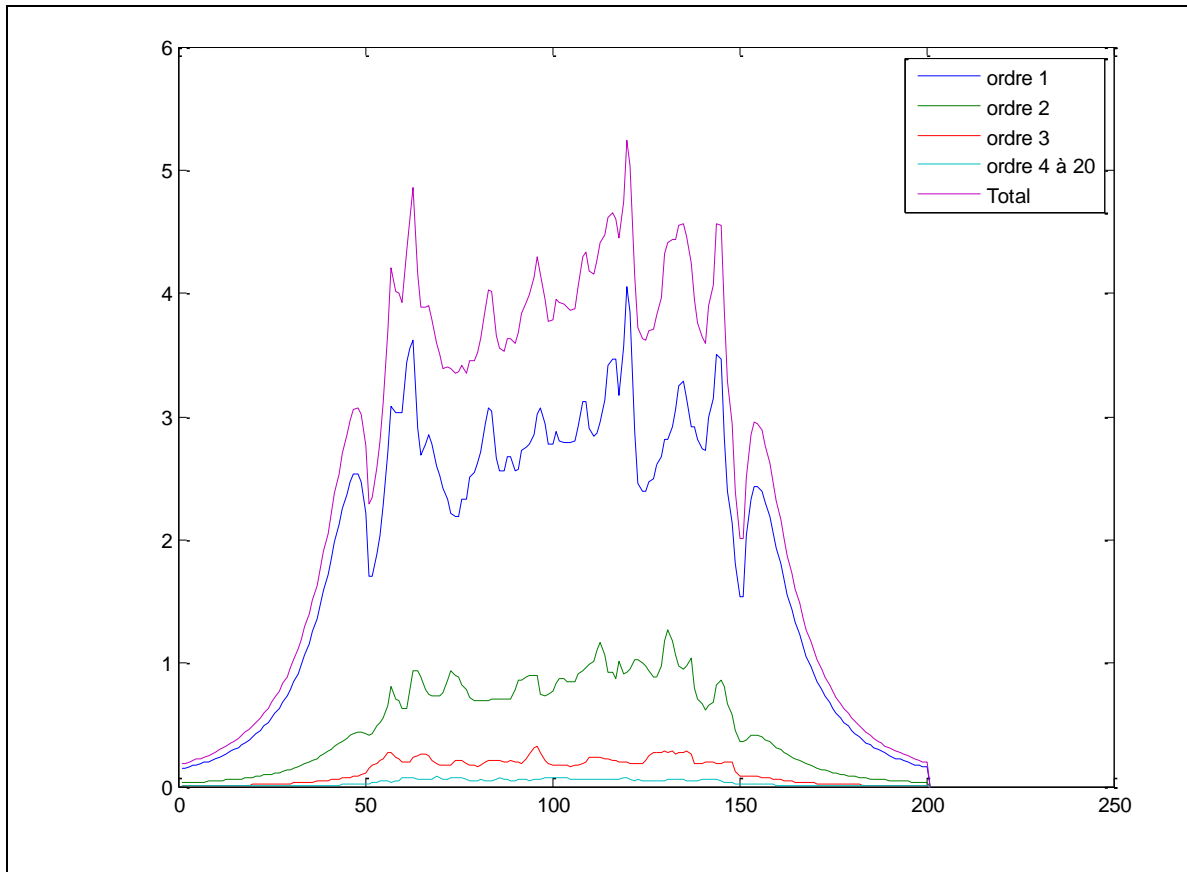


Figure 12: Scatter profiles for different orders obtained with VXI and Monte-Carlo sampling technique.

6. Conclusions

Analytical scatter calculations coupled with a geometric sampling are a viable alternative for transmitting imaging and small wall thicknesses, where lower order scattering is dominant. Such a method is also very useful for non-conventional method like Compton tomography for example.

Using a Monte Carlo sampling approach, the analytical scatter model provides scatter predictions for any scattering order. Our first results with this approach demonstrate the feasibility of this concept, but also show higher sampling noise as a side-effect of the Monte Carlo sampling. This noise can be reduced increasing the number of sampling points.

A number of improvements are possible, in particular a sampling filter, eliminating sample points too close to the detector, which generate peaks in the scatter profile. As part of Radiola's project, further comparisons will be made to determine if the inherent advantages of Monte Carlo sampling outweigh the inconvenience of higher sampling noise while keeping the advantage of computation time. Once results of analytical scatter calculations will be definitively validated and conclusive this option will be integrated onto CIVA platform.

Bibliography

- [1] O. Bremnes, B. Chassignole, O. Dupond, A. Schumm, «Experimental and simulation studies of radiographic inspections of pressure vessel reactors», ECNDT, 2006.
- [2] J. Tabary, P. Hugonnard, and F. Mathy, "SINDBAD: a realistic multi-purpose and scalable X-ray simulation tool for NDT applications", Proc. International Symposium on Digital industrial Radiology, Lyon, France, June 2007.
- [3] G.-R. Jaenisch, C. Bellon, U. Samadurau, M. Zhukovsky, and S. Podoliako, "Monte Carlo Simulation Tool with CAD Interface" in *Review of Progress in QNDE. 25*. edited by D. O. Thompson and D. E. Chimenti. AIP Conference Proceedings vol. 820. American Institute of Physics. Melville. NY (2006). pp. 574-581.
- [4] Ph. DUVAUCHELLE, Nicolas FREUD, Valérie KAFTANDJIAN, Daniel BABOT - A computer code to simulate X-ray imaging techniques. *Nuclear Instruments and Methods in Physics Research B. 2000. - Pages245-258*
- [5] N. Freud, Ph. DUVAUCHELLE and D. Babot, New Developments in Virtual X-ray Imaging: Fast Simulation Using a Deterministic Approach, review of progress in quantitative nondestructive evaluation. *Volume 22. AIP Conference Proceedings, Volume 657, Pages 553-560 (2003)*
- [6] Ph. Duvauchelle, J. Berthier, New developments in analytical calculation of first order scattering for 3D complex objects, DIR 2007 - International Symposium on Digital industrial Radiology and Computed Tomography, June 25-27, 2007, Lyon, France
- [7] A.Bonnin, Ph. Duvauchelle, V.Kaftandjian, P. Ponard, A simulation tool for Compton scattering imaging: application to illicit substances detection, FINEX, Chypre, 13-16 mai 2008.
- [8] R. Fernandez, A. Schumm, J. Tabary, P. Hugonnard, Simulation studies of radiographic inspections with CIVA – WCNDT, Shanghai 2008.